

About contact force-laws for cohesive frictional materials in 2D and 3D

Stefan Luding

Institute for Computerphysics (ICP), University of Stuttgart,
Pfaffenwaldring 27, 70569 Stuttgart, Germany, and
Particle Technology, Nanostructured Materials, DelftChemTech,
TUDelft, Julianalaan 136, 2628 BL Delft, Netherlands

Abstract

Ultrafine, cohesive powders are the subject of the joint research project. While shear experiments and contact force measurements were performed by the project partners, the realistic contact force models were developed in a common effort. The algorithms for their implementation are presented here, involving elastic-plastic repulsion, dissipation, adhesion, friction as well as rolling- and torsion-resistance.

In model powder systems, the effect of the contact properties on an isotropic, homogeneous compaction test is discussed with respect to the packing densities. With contact forces involving sliding, rolling and torsion frictions, packing volume fractions down to 0.42 were achieved. Some longer ranged van der Waals adhesion forces added to the contact forces can lead to volume fractions considerably smaller, and to fractal-like agglomerates.

Keywords

granular materials, molecular dynamics (MD) and discrete element model (DEM) force-laws, friction, rolling- and torsion resistance, adhesion, plastic deformation, low density compaction

1 Introduction

Ultrafine, cohesive powders show peculiar flow behavior, including macroscopic cohesion and a yield stress that has to be reached, before flow sets in. Besides many experiments, Molecular Dynamics (MD) or Discrete Element Models (DEM), which solve the equations of motion for all particles in a system, are used to understand these granular media. While experiments and continuum theory deal with macroscopic material parameters, for the particle simulations, the (microscopic) contact forces are the only physical laws that have to be defined beforehand [3, 8, 9, 13, 20].

1.1 Project Overview

The project “Modellierung der Scherdynamik kohäsiver, feindisperser Partikelsysteme” in the framework of the DFG research group “Verhalten Granularer Medien” was dealing with shear experiments [32–35], constitutive modeling and [14–17, 19, 23, 26], discrete element simulations [2, 6, 7, 16, 18, 34, 35]. These three subjects are also addressed on pages 83, 99, and 143 of this proceedings, respectively. Tools to perform a so-called micro-macro transition are examined [14, 36] with

the goal to relate the macroscopic flow behavior to the microscopic contact properties. The contact force measurement, see [11] and the paper on page 89 of this proceeding, and the contact force models [13, 20, 23, 24] are essential for the DEM simulations and are the main subject of this paper, see also the papers on pages 75, 83, and 89 of this book. This involves advanced contact models for elasto-plastic, adhesive normal forces and friction, rolling- and torsion-resistance; contact models for temperature dependent sintering are discussed elsewhere [24].

1.2 Contact Modeling

For powders, as an example, the particle properties and interaction laws are inserted into a discrete particle molecular dynamics and lead to the collective behavior of the dissipative, frictional, adhesive many-particle system. From the particle simulation, one can extract, e.g., the coordination number or the pressure of the system as a function of density, but also velocity gradient, viscosity and other macroscopic material properties. In the following, normal interactions, like adhesion and elasto-plastic contact deformations are introduced as well as friction, rolling- and torsion re-

sistance in tangential direction. All models are discussed for disks and spherical model particles. Examples of a compression test are presented for which the previously defined contact model parameters are varied and the compaction process is affected – see also the closely related project “Verdichtung und mechanische Eigenschaften von kohäsiven Schüttgütern”.

2 Soft Particle Molecular Dynamics (MD)

Particle simulations like MD are also referred to as discrete element models (DEM) [4, 5, 10, 12, 29, 30, 36]. They complement experiments on small “representative volume elements” (REVs). Alternative methods like contact dynamics (CD) or cell- and lattice gas-methods are not discussed here.

2.1 Discrete Particle Model

The elementary units of granular materials are mesoscopic grains, which deform under stress. Since the realistic modeling of the deformations of the particles is much too complicated, we relate the interaction force to the overlap δ of two particles, see Fig. 1. In tangential direction, the forces also depend on the tangential displacement since the beginning of the contact. Note that the evaluation of the inter-particle forces based on the overlap may not be sufficient to account for the inhomogeneous stress distribution inside the particles and possible multi-contact effects. Consequently, the results presented here are of the same quality as the simplifying assumptions about the force-overlap relations made.

2.2 Equations of Motion

If all forces \mathbf{f}_i acting on the particle i , either from other particles, from boundaries or from external forces, are known, the problem is reduced to the integration of Newton’s equations of motion for the translational and rotational degrees of freedom:

$$m_i \frac{d^2}{dt^2} \mathbf{r}_i = \mathbf{f}_i + m_i \mathbf{g}, \quad \text{and} \quad I_i \frac{d^2}{dt^2} \boldsymbol{\varphi}_i = \mathbf{q}_i \quad (1)$$

with the mass m_i of particle i , its position \mathbf{r}_i , the total force $\mathbf{f}_i = \sum_c \mathbf{f}_i^c$ acting on it due to contacts with other particles or with the walls, the acceleration due to volume forces like gravity \mathbf{g} , the particles moment of inertia I_i , its angular velocity $\boldsymbol{\omega}_i = d\boldsymbol{\varphi}_i/dt$ and the total torque $\mathbf{q}_i = \mathbf{q}_i^{\text{friction}} + \mathbf{q}_i^{\text{rolling}} + \mathbf{q}_i^{\text{torsion}}$, as defined below.

The equations of motion are thus a system of $\mathcal{D} + \mathcal{D}(\mathcal{D} - 1)/2$ coupled ordinary differential equations to be solved in \mathcal{D} dimensions, with $\mathcal{D} = 2$ or

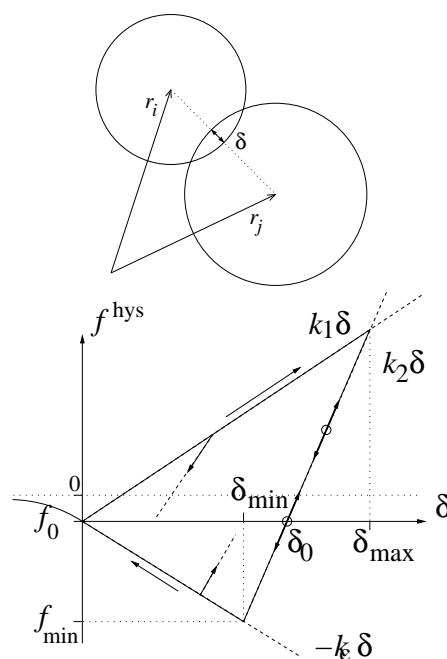


Figure 1: (Top) Two particle contact with overlap δ in normal direction. (Bottom) Schematic graph of the piecewise linear, hysteretic, adhesive force-displacement model in normal direction.

$\mathcal{D} = 3$. With tools from numerical integration, as nicely described in textbooks as [1, 27], this is a straightforward exercise. The typically short-ranged interactions in granular media, allow for further optimization by using linked-cell (LC) or alternative methods in order to make the neighborhood search more efficient. In the case of long-range interactions, (e.g., charged particles or van der Waals type forces) this is not possible anymore, so that either a cut-off or more advanced methods for optimization have to be applied – for the sake of brevity, we use a cut-off for van der Waals forces and the LC method below.

2.3 Normal Contact Force Laws

Two spherical particles i and j , with radii a_i and a_j , respectively, interact only if they are in contact so that their overlap

$$\delta = (a_i + a_j) - (\mathbf{r}_i - \mathbf{r}_j) \cdot \mathbf{n} \quad (2)$$

is positive, $\delta > 0$, with the unit vector $\mathbf{n} = \mathbf{n}_{ij} = (\mathbf{r}_i - \mathbf{r}_j)/|\mathbf{r}_i - \mathbf{r}_j|$ pointing from j to i . The force on particle i , from particle j , at contact c , can be decomposed into a normal and a tangential part as $\mathbf{f}^c := \mathbf{f}_i^c = f^n \mathbf{n} + f^t \mathbf{t}$, where $\mathbf{n} \cdot \mathbf{t} = 0$. The tangential force leads to a torque as well as rolling and torsion, as discussed below.

2.3.1 Linear Normal Contact Model

The simplest normal contact force model, which takes into account excluded volume and dissipa-

tion, involves a linear repulsive and a linear dissipative force

$$f^n = k\delta + \gamma_0 v_n, \quad (3)$$

with a spring stiffness k , a viscous damping γ_0 , and the relative velocity in normal direction $v_n = -\mathbf{v}_{ij} \cdot \mathbf{n} = -(\mathbf{v}_i - \mathbf{v}_j) \cdot \mathbf{n} = \dot{\delta}$.

This so-called linear spring dashpot (LSD) model allows to view the particle contact as a damped harmonic oscillator, for which the half-period of a vibration around an equilibrium position with a certain contact force, can be computed [13]. The typical response time on the contact level is

$$t_c = \frac{\pi}{\omega}, \quad \text{with} \quad \omega = \sqrt{(k/m_{12}) - \eta_0^2}, \quad (4)$$

the eigenfrequency of the contact, the rescaled damping coefficient $\eta_0 = \gamma_0/(2m_{ij})$, and the reduced mass $m_{ij} = m_i m_j / (m_i + m_j)$. From the solution of the equation of a half period of the oscillation, one also obtains the coefficient of restitution

$$r = v'_n / v_n = \exp(-\pi\eta_0/\omega) = \exp(-\eta_0 t_c), \quad (5)$$

which quantifies the ratio of normal relative velocities after (primed) and before (unprimed) the collision. For a more detailed discussion of this and other, more realistic, non-linear contact models, see Ref. [13].

The contact duration in Eq. (4) is also of practical technical importance, since the integration of the equations of motion is stable only if the integration time-step Δt_{MD} is much smaller than t_c . Note that t_c depends on the magnitude of dissipation: In the extreme case of an overdamped spring, t_c can become very large (which would render the contact behavior artificial [21]). Therefore, the use of neither too weak nor too strong dissipation is recommended.

2.3.2 Adhesive, Elasto-Plastic Contacts

Here we apply a variant of the linear hysteretic spring model [13, 31, 37], as an alternative to the frequently applied spring-dashpot models. This model is the simplest version of some more complicated nonlinear-hysteretic force laws [28, 31, 37, 38], which reflect the fact that at the contact point, plastic deformations may take place and attractive (adhesive) forces exist. The adhesive, plastic (hysteretic) force-law can be written as

$$f^{\text{hys}} = \begin{cases} k_1 \delta & \text{if } k_2(\delta - \delta_0) \geq k_1 \delta \\ k_2(\delta - \delta_0) & \text{if } k_1 \delta > k_2(\delta - \delta_0) > -k_c \delta \\ -k_c \delta & \text{if } -k_c \delta \geq k_2(\delta - \delta_0) \end{cases} \quad (6)$$

with $k_1 \leq k_2$, see Fig. 1. The first and the third case are for un- and re-loading, respectively, while the second case is for both un- and re-loading and will be discussed in more detail below. During the initial loading the force increases linearly with the overlap δ , until the maximum overlap δ_{max} is reached (which has to be kept in memory as a history parameter). The line with slope k_1 thus defines the maximum force possible for a given δ . During unloading the force drops from its value at δ_{max} down to zero at overlap $\delta_0 = (1 - k_1/k_2)\delta_{\text{max}}$, on the line with slope k_2 , so that δ_0 resembles the *plastic contact deformation*. Reloading at any instant leads to an increase of the force along the line with slope k_2 , until the maximum force is reached; for still increasing δ , the force follows again the line with slope k_1 and δ_{max} has to be adjusted accordingly.

Unloading below δ_0 leads to negative, *attractive forces* until the minimum force $-k_c \delta_{\text{min}}$ is reached at the overlap $\delta_{\text{min}} = (k_2 - k_1)\delta_{\text{max}} / (k_2 + k_c)$. This minimum force, i.e., the maximum attractive force, is obtained as a function of the model parameters k_1 , k_2 , k_c , and the history parameter δ_{max} . Further unloading leads to attractive forces $f^{\text{hys}} = -k_c \delta$ on the adhesive branch with slope $-k_c$. The highest possible attractive force, for given k_1 and k_2 , is reached for $k_c \rightarrow \infty$, so that $f_{\text{max}}^{\text{hys}} = -(k_2 - k_1)\delta_{\text{max}}$. Since this would lead to a discontinuity at $\delta = 0$, it is avoided by using finite k_c .

The lines with slope k_1 and $-k_c$ define the range of possible force values and departure from these lines takes place in the case of loading and unloading, respectively. Between these two extremes, unloading and reloading follow the line with slope k_2 . Possible equilibrium states are indicated as circles in Fig. 1, where the upper and lower circle correspond to a pre-stressed and stress-free state, respectively. Small perturbations lead, in general, to small deviations along the line with slope k_2 as indicated by the arrows in Fig. 1.

A non-linear un/reloading behavior would be more realistic, however, due to a lack of detailed experimental informations, the piece-wise linear model is used as a compromise. One reasonable refinement, which accounts for an *increasing stiffness* with deformation, is a k_2 value dependent on the maximum overlap. This also implies relatively small and large plastic deformations for weak and strong contact forces, respectively. The model, as proposed recently [25], requires an additional model parameter,

$$\delta_{\text{max}}^* = \frac{k_2}{k_2 - k_1} \phi_f \frac{a_1 + a_2}{2}, \quad (7)$$

with the dimensionless plasticity depth, ϕ_f , defined relative to the average radius. If the pen-

etration is larger than a fraction ϕ_f of the (average) particle radius, the constant stiffness k_2 is used. Note that a limit to the slope k_2 is needed for practical reasons. If k_2 would not be limited, the contact duration could become very small so that the time step would have to be reduced below reasonable values.

For smaller penetration, $k_2(\delta_{\max})$ interpolates between k_1 and k_2 :

$$k_2(\delta_{\max}) = \begin{cases} k_2 & \text{if } \delta_{\max}/\delta_{\max}^* \geq 1 \\ k_1 + (k_2 - k_1)\delta_{\max}/\delta_{\max}^* & \text{if } \delta_{\max}/\delta_{\max}^* < 1 \end{cases}, \quad (8)$$

and the constant k_2 in Eq. (6) is replaced by the variable $k_2(\delta_{\max})$ from Eq. (8).

While in the case of collisions of particles with large relative velocities – and thus large deformations – dissipation takes place due to the hysteretic nature of the force-law, reasonably strong dissipation of small amplitude deformations is achieved by adding the viscous, velocity dependent dissipative force from Eq. (3) to the hysteretic force, such that $f^n = f^{\text{hys}} + \gamma_0 v_n$.

In summary, the adhesive, plastic, hysteretic normal contact model contains the five parameters k_1 , k_2 , k_c , ϕ_f , and γ_0 that respectively account for loading-reloading-stiffness and plastic deformation, adhesion, plastic overlap-range of the model, and viscous dissipation¹.

2.3.3 Long Range Normal Forces

Medium range van der Waals forces can be taken into account in addition to the hysteretic force such that $f^n = f^{\text{hys}} + \gamma_0 v_n + f^{\text{vdW}}$ with, for example, a Lennard-Jones Potential, leading to the force as function of distance:

$$f^{\text{vdW}}(r) = -(4\varepsilon/r_0) [6(r_0/r)^7 - 12(r_0/r)^{13}]. \quad (9)$$

In order to have a continuous force-displacement relation and to limit the range of the force, usually, a cut-off is introduced, so that

$$f^{\text{vdW}} = f^{\text{vdW}}(r) - f^{\text{vdW}}(r_c), \quad \text{for } r < r_c, \quad (10)$$

and $f^{\text{vdW}} = 0$ elsewhere. The new parameters necessary for this force are an energy scale ε , a typical length scale r_0 and the cut-off length r_c . As long as r_c is not too large as compared to the particle diameter, the neighbourhood-search methods for short range interactions still can be still applied – only the linked cells have to be larger than twice the cut-off radius. When r_0 is smaller

than the particle diameter, the repulsive part of the force becomes irrelevant due to the repulsive contact model.

2.4 Tangential Contact Force Laws

For the tangential degrees of freedom, there are three different force- and torque-laws to be implemented: (i) friction, (ii) rolling resistance, and (iii) torsion resistance.

2.4.1 Sliding

For sliding and static *friction*, the relative tangential velocity of the contact points,

$$\mathbf{v}_t = \mathbf{v}_{ij} - \mathbf{n}(\mathbf{n} \cdot \mathbf{v}_{ij}), \quad (11)$$

is to be considered for the force and torque computations in subsection 2.5, with the total relative velocity of the particle surfaces at the contact

$$\mathbf{v}_{ij} = \mathbf{v}_i - \mathbf{v}_j + a'_i \mathbf{n} \times \boldsymbol{\omega}_i + a'_j \mathbf{n} \times \boldsymbol{\omega}_j, \quad (12)$$

with the corrected radius relative to the contact point $a'_\alpha = a_\alpha - \delta/2$. The forces on the contacting particles are computed from the accumulated sliding of the contact points along each other, as described in detail in subsection 2.5.1. Both frictional force and torque are active when the two particles are rotating in parallel and are sliding along each other.

In general, the two particles are rotating together² with an angular velocity $\boldsymbol{\omega}_0 = \boldsymbol{\omega}_0^n + \boldsymbol{\omega}_0^t$, with the tangential plane component

$$\boldsymbol{\omega}_0^t = \frac{\mathbf{n} \times (\mathbf{v}_i - \mathbf{v}_j)}{a'_i + a'_j}. \quad (13)$$

Inserting $\boldsymbol{\omega}_i = \boldsymbol{\omega}_j = \boldsymbol{\omega}_0^t$, from Eq. (13), into Eq. (12) leads to zero sliding velocity, proving that the formulation is objective, i.e., independent of a rotation of the system of reference.

Since action should be equaled by reaction, the tangential forces are equally strong, but opposite, i.e., $\mathbf{f}_j^t = -\mathbf{f}_i^t$, while the corresponding torques are parallel but not necessarily equal in magnitude: $\mathbf{q}_i^{\text{friction}} = -a'_i \mathbf{n} \times \mathbf{f}_i$, and $\mathbf{q}_j^{\text{friction}} = (a'_j/a'_i) \mathbf{q}_i^{\text{friction}}$. Note that tangential forces and torques *together* conserve the total angular momentum

$$\mathbf{L}_{ij} = \mathbf{L}_i + \mathbf{L}_j + m_i r_{i\text{cm}}^2 \boldsymbol{\omega}_0 + m_j r_{j\text{cm}}^2 \boldsymbol{\omega}_0, \quad (14)$$

with the rotational contributions $\mathbf{L}_\alpha = I_\alpha \boldsymbol{\omega}_\alpha$, for $\alpha = i, j$, and the distances $r_{\alpha\text{cm}} = |\mathbf{r}_\alpha - \mathbf{r}_{\text{cm}}|$ from

¹The hysteretic model contains the linear contact model as special case $k_1 = k_2 = k$

²Rotation can be either due to a rotation of the reference system or because of a non-central collision.

the particle centers to the center of mass $\mathbf{r}_{\text{cm}} = (m_i \mathbf{r}_i + m_j \mathbf{r}_j) / (m_i + m_j)$, see Ref. [13]. The change of angular momentum consists of the change of particle spins (first term) and of the change of the angular momentum of the two masses rotating about their common center of mass (second term):

$$\frac{d\mathbf{L}_{ij}}{dt} = \mathbf{q}_i^{\text{friction}} \left(1 + \frac{a'_j}{a'_i} \right) + (m_i r_{\text{icm}}^2 + m_j r_{\text{jcm}}^2) \frac{d\boldsymbol{\omega}_0}{dt}, \quad (15)$$

which both contribute, but exactly cancel each other, since

$$\mathbf{q}_i^{\text{friction}} \left(1 + \frac{a'_j}{a'_i} \right) = -(a'_i + a'_j) \mathbf{n} \times \mathbf{f}_i \quad (16)$$

and

$$(m_i r_{\text{icm}}^2 + m_j r_{\text{jcm}}^2) \frac{d\boldsymbol{\omega}_0}{dt} = \quad (17)$$

$$m_{ij} (\mathbf{r}_i - \mathbf{r}_j)^2 \frac{\mathbf{n} \times \left(\frac{d}{dt} \mathbf{v}_i - \frac{d}{dt} \mathbf{v}_j \right)}{a'_i + a'_j} =$$

$$m_{ij} (a'_i + a'_j) \mathbf{n} \times \left(\frac{\mathbf{f}_i}{m_i} - \frac{\mathbf{f}_j}{m_j} \right) =$$

$$(a'_i + a'_j) \mathbf{n} \times \mathbf{f}_i,$$

when the relations for force, angular momentum, etc., as introduced above are inserted.

2.4.2 Rolling

For *rolling resistance*, a rolling velocity

$$\mathbf{v}_r^0 = -a'_i \mathbf{n} \times \boldsymbol{\omega}_i + a'_j \mathbf{n} \times \boldsymbol{\omega}_j, \quad (18)$$

defined just in simple-minded analogy to the sliding velocity [20], is not objective in general [9] – it is objective, however, in the special cases of (i) equal-sized particles [20] and (ii) for a particle with radius a_i , rolling on a fixed flat surface with $a'_j \boldsymbol{\omega}_j = 0$.

Since the rolling velocity quantifies the distance the two surfaces roll over each other (without sliding) it is equal for both particles by definition. An *objective rolling velocity* is obtained by replacing the particle radii in Eq. (18) by the reduced radius, $a'_{ij} = a'_i a'_j / (a'_i + a'_j)$, so that

$$\mathbf{v}_r = -a'_{ij} (\mathbf{n} \times \boldsymbol{\omega}_i - \mathbf{n} \times \boldsymbol{\omega}_j). \quad (19)$$

This definition is objective since any common rotation of the two particles vanishes by construction.

Furthermore, it is equivalent to Eq. (18) for a single particle on a flat surface with $a'_{ij} = a'_i$ and $\boldsymbol{\omega}_j = 0$. For the special case of equal sized particles, Eq. (18) and Eq. (19) differ by a factor of two – the former accounts double for the rolling distance and velocity – so that Eq. (19) appears more reasonable. A more detailed discussion of this and alternative discussions and interpretations is beyond the scope of this paper, rather see [9] and the references therein.

The rolling velocity will activate torques, acting against the rolling motion, when two particles are rotating anti-parallel with spins in the tangential plane. These torques act against rolling and are equal in magnitude and opposite in direction, i.e., $\mathbf{q}_i^{\text{rolling}} = -\mathbf{q}_j^{\text{rolling}} = a_{ij} \mathbf{n} \times \mathbf{f}_r$, with the quasi-force \mathbf{f}_r . This quasi-force is computed in analogy to the friction force as function of the rolling velocity \mathbf{v}_r in subsection 2.5.2; the quasi-forces for both particles are equal and do not act on the centers of mass. Therefore, the total momenta (translational and angular) are conserved.

2.4.3 Torsion

For *torsion resistance*, the relative spin along the normal direction

$$\mathbf{v}_o = a_{ij} (\mathbf{n} \cdot \boldsymbol{\omega}_i - \mathbf{n} \cdot \boldsymbol{\omega}_j) \mathbf{n}, \quad (20)$$

is to be considered, which activates torques when two particles are rotating anti-parallel with spins parallel to the normal direction. Torsion is not activated by a common rotation of the particles $\boldsymbol{\omega}_0 = (\boldsymbol{\omega}_i + \boldsymbol{\omega}_j) / 2$, which makes the torsion resistance objective.

The torsion torques are equal in magnitude and directed in opposite direction, i.e., $\mathbf{q}_i^{\text{torsion}} = -\mathbf{q}_j^{\text{torsion}} = a_{ij} \mathbf{f}_o$, with the quasi-force \mathbf{f}_o , computed from the torsion velocity in subsection 2.5.3, and also does not change the translational momentum. Like for rolling, the torsion torques conserve the total angular momentum.

2.4.4 Summary

The implementation of the tangential force computations for \mathbf{f}_t , \mathbf{f}_r , and \mathbf{f}_o as based on \mathbf{v}_t , \mathbf{v}_r , and \mathbf{v}_o , respectively, is assumed to be *identical*, i.e., even the same subroutine is used, but with different parameters as specified below. The difference is that friction leads to a force in the tangential plane (changing both translational and angular momentum), while rolling- and torsion-resistance lead to quasi-forces – and thus to torques only – changing the particles' angular, but not the translational momentum. For more details on tangen-

tial contact models, friction, rolling and torsion, see Refs. [3, 8, 9, 20].

2.5 The tangential contact model

The unique feature of this tangential contact model is the fact that a single procedure (sub-routine) can be used to compute either sliding, rolling, or torsion resistance. The subroutine needs a velocity as input and returns the respective force or quasi-force. Below, the sliding/sticking friction model will be introduced in detail, while the rolling and torsion resistance then only have to be discussed where different from the sliding model, i.e., with respect to the material parameters and the action of forces and torques.

2.5.1 Sliding frictional Model

The tangential force is coupled to the normal force via Coulombs law, i.e. $f^t \leq \mu^s f^n$, where for the limit case one has dynamic friction with $f^t = \mu^d f^n$. The dynamic and the static friction coefficients follow, in general, the relation $\mu^d \leq \mu^s$. The static situation requires an elastic spring in order to allow for a restoring force, i.e. a non-zero remaining tangential force in static equilibrium due to activated Coulomb friction.

If a repulsive contact is established, and thus one has $f^n > 0$, the tangential force is active. In the presence of adhesion, Coulombs law has to be slightly modified in so far that f^n is replaced by $f^n + k_c \delta$. With other words, the reference criterion for a contact is no longer the zero force level, but it is the adhesive, attractive force level along $-k_c \delta$. Coulombs law in the presence of adhesion thus reads $f^t \leq \mu^s (f^n + k_c \delta)$ for the static case and $f^t = \mu^d (f^n + k_c \delta)$ for the dynamic, sliding case.

If a contact is active, one has to project (or better rotate) the tangential spring into the actual tangential plane, since the frame of reference of the contact may have rotated since the last time-step. The new tangential spring is:

$$\boldsymbol{\xi} = \boldsymbol{\xi}' - \mathbf{n}(\mathbf{n} \cdot \boldsymbol{\xi}') , \quad (21)$$

where $\boldsymbol{\xi}'$ is the old spring from the last iteration. This action is relevant only for an already existing spring; if the spring is new, the tangential spring-length is zero anyway, however, its change is well defined even for the first, initiation step. In order to compute the changes of the tangential spring, a tangential test-force is first computed as the sum of the tangential spring force and a tangential viscous force (in analogy to the normal viscous force)

$$\mathbf{f}_0^t = -k_t \boldsymbol{\xi} - \gamma_t \mathbf{v}_t , \quad (22)$$

with the tangential spring stiffness k_t , the tangential dissipation parameter γ_t , and \mathbf{v}_t from Eq. (11). As long as $|\mathbf{f}_0^t| \leq f_C^s$, with $f_C^s = \mu^s (f^n + k_c \delta)$, one has static friction and, on the other hand, if the limit $|\mathbf{f}_0^t| > f_C^s$ is reached, sliding friction is active with magnitude $f_C^d = \mu^d (f^n + k_c \delta)$. (As soon as $|\mathbf{f}_0^t|$ becomes smaller than f_C^d , static friction is active again.) In the former, static case, the tangential spring is incremented

$$\boldsymbol{\xi}' = \boldsymbol{\xi} + \mathbf{v}_t \Delta t_{\text{MD}} , \quad (23)$$

to be used in the next iteration in Eq. (21), and the force $\mathbf{f}^t = \mathbf{f}_0^t$ from Eq. (22) is used. In the latter, sliding case, the tangential spring is adjusted to a length which is consistent with Coulombs condition

$$\boldsymbol{\xi}' = -\frac{1}{k_t} f_C^d \mathbf{t} , \quad (24)$$

with the tangential unit vector, $\mathbf{t} = \mathbf{f}_0^t / |\mathbf{f}_0^t|$, defined by Eq. (22), and thus the magnitude of the Coulomb force is used. Inserting $\boldsymbol{\xi}'$ from Eq. (24) into Eq. (22) leads to $\mathbf{f}_0^t \approx f_C^d \mathbf{t} - \gamma_t \mathbf{v}_t$. Note that \mathbf{f}_0^t and \mathbf{v}_t are not necessarily parallel in three dimensions. However, the mapping in Eq. (24) works always, rotating the new spring such that the direction of the frictional force is unchanged and, at the same time, limiting the spring in length according to Coulombs law. In short notation the tangential contact law reads

$$\mathbf{f}^t = f^t \mathbf{t} = +\min(f_C, |\mathbf{f}_0^t|) \mathbf{t} , \quad (25)$$

where f_C follows the static/dynamic selection rules described above. The torque on a particle due to frictional forces at this contact is $\mathbf{q}^{\text{friction}} = \mathbf{l}_i^c \times \mathbf{f}_i^c$, where \mathbf{l}_i^c is the branch vector, connecting the center of the particle with the contact point.

The four parameters for the friction law are k_t , μ_s , $\phi_d = \mu_d / \mu_s$, and γ_t , accounting for tangential stiffness, the static friction coefficient, the dynamic friction ratio, and tangential viscosity, respectively. Note that the tangential force described above is identical to the classical Cundall-Strack spring only in the limits $\mu = \mu^s = \mu^d$, i.e., $\phi_d = 1$, and $\gamma_t = 0$. The sequence of computations and the definitions and mappings into the tangential direction can be used in three dimensions as well as in two.

2.5.2 Rolling Resistance Model

The three new parameters for rolling resistance are k_r , μ_r , and γ_r , while ϕ_d is used from the friction law. The new parameters account for rolling stiffness, the static rolling “friction” coefficient, and rolling viscosity, respectively. In the subroutine

called, the rolling velocity \mathbf{v}_r is used instead of \mathbf{v}_t and the computed quasi-force \mathbf{f}_r is used to compute the torques, $\mathbf{q}^{\text{rolling}}$, on the particles, see above.

2.5.3 Torsion Resistance Model

The three new parameters for rolling resistance are k_o , μ_o , and γ_o , while ϕ_d is used from the friction law. The new parameters account for torsion stiffness, the static torsion “friction” coefficient, and torsion viscosity, respectively. In the subroutine, the torsion velocity \mathbf{v}_o is used instead of \mathbf{v}_t and the projection is a projection along the normal unit-vector. The computed quasi-force \mathbf{f}_o is then used to compute the torques, $\mathbf{q}^{\text{torsion}}$, on the particles.

2.6 Background Friction

Note that the viscous dissipation takes place in a two-particle contact. In the bulk material, where many particles are in contact with each other, this dissipation mode is very inefficient for long-wavelength cooperative modes of motion [21, 22]. Therefore, an additional damping with the background can be introduced, so that the total force on particle i is

$$\mathbf{f}_i = \sum_j (f^n \mathbf{n} + f^t \mathbf{t}) - \gamma_b \mathbf{v}_i, \quad (26)$$

and the total torque

$$\mathbf{q}_i = \sum_j (\mathbf{q}^{\text{friction}} + \mathbf{q}^{\text{rolling}} + \mathbf{q}^{\text{torsion}}) - \gamma_{br} a_i^2 \boldsymbol{\omega}_i, \quad (27)$$

with the damping artificially enhanced in the spirit of a rapid relaxation and equilibration. The sum in Eqs. (26) and (27) takes into account all contact partners j of particle i , but the background dissipation can be attributed to the medium between the particles. Note that the effect of γ_b and γ_{br} should be checked for each simulation in order to exclude artificial over-damping.

3 Compaction Simulation Results

In this section, a compression test is presented, where the particles are positioned on a square-lattice in a cubic system with periodic boundary conditions, in order to avoid wall effects. The system is first allowed to evolve to a disordered state, by attributing random velocities to all particles. The density is then increased by slowly increasing the particle size while the system volume $V = L^3$, with $L = 0.025$ m, is kept constant. During the simulation, the particles are growing and density, coordination number and energies are reported.

3.1 Model Parameters

The systems examined in the following contain $N = 1728$ particles with equal radii a . In the simulation, the radii change according to the relation

$$\frac{da}{dt} = g_a, \quad (28)$$

with the growth rate $g_a = 2.10^{-7} \text{ ms}^{-1}$, if not explicitly specified. The growth is stopped when a target volume fraction $\nu = NV(a)/V$ is reached, with the particle volume $V(a) = (4/3)\pi a^3$. The particle mass $m(a) = \rho V(a)$, with the material density ρ , changes with the radius during the growth period.

| Property | Symbol |
|----------------------------------|------------------------|
| Time Unit | t_u |
| Initial particle radius | a_0 |
| Growth rate | g_a |
| Particle radius | $a(t) = a_0 + g_a t$ |
| Material density | ρ |
| Elastic stiffness | $k = k_2$ |
| Plastic stiffness | k_1/k |
| Adhesion “stiffness” | k_c/k |
| Friction stiffness | k_t/k |
| Rolling stiffness | k_r/k |
| Torsion stiffness | k_o/k |
| Plasticity depth | ϕ_f |
| Coulomb friction coefficient | $\mu = \mu_d = \mu_s$ |
| Dynamic to static Friction ratio | $\phi_d = \mu_d/\mu_s$ |
| Rolling “friction” coefficient | μ_r |
| Torsion “friction” coefficient | μ_o |
| Normal viscosity | $\gamma = \gamma_n$ |
| Friction viscosity | γ_t/γ |
| Rolling viscosity | γ_r/γ |
| Torsion viscosity | γ_o/γ |
| Background viscosity | γ_b/γ |
| Background viscous torque | γ_{br}/γ |
| Lennard Jones energy | ε |
| Lennard Jones distance | $r_0/(2a)$ |
| Lennard Jones cut-off | $r_c/(2a)$ |

Table 1: The microscopic contact model parameters.

A typical set of material parameters is given in table 2. The choice of numbers and units is such that the particles correspond to micro-meter sized, (overly) soft aluminum spheres. The stiffness magnitude (this is not the material bulk modulus, but a contact property) used thus appears much too small for this material – however, dependent on the volume fraction (or the external) pressure, the material deformation (overlap) can be realistic if the simulations are performed so slow that rate effects are small and overlaps are not becoming too

| Symbol | Values | t -rescaled |
|------------------------|------------------------------------|-----------------------------------|
| t_u | 1 s | 1 μ s |
| a_0 | 0.5 μ m | |
| g_a | 0.2 μ m/s | 0.2 m/s |
| $a(t) = a_0 + g_a t$ | | |
| ρ | 2000 kg/m ³ | |
| $k = k_2$ | 10 ⁻⁷ kg/s ² | 10 ⁵ kg/s ² |
| k_1/k | 0.2 | |
| k_c/k | 1.0 | |
| k_t/k | 0.2 | |
| k_r/k | 0.2 | |
| k_o/k | 0.2 | |
| ϕ_f | 0.05 | |
| $\mu = \mu_d = \mu_s$ | 1 | |
| $\phi_d = \mu_d/\mu_s$ | 1 | |
| μ_r | 0.1 | |
| μ_o | 0.1 | |
| $\gamma = \gamma_n$ | 2 10 ⁻¹³ kg/s | 2 10 ⁻⁷ kg/s |
| γ_t/γ | 0.25 | |
| γ_r/γ | 0.25 | |
| γ_o/γ | 0.25 | |
| γ_b/γ | 0.10 | |
| γ_{br}/γ | 0.05 | |
| ε | 0. 10 ⁻¹⁵ J | 0. 10 ⁻³ J |
| $r_0/(2a)$ | 0.5 | |
| $r_c/(2a)$ | 1.5 | |

Table 2: The microscopic material parameters used if not explicitly specified. The third column contains those values that are different due to rescaling of the unit of time, i.e., when seconds are read as μ s.

large. A simple rescaling of time brings the material parameters into the reasonable range – see rightmost column in table 2.

Using the parameter $k = k_2$ in Eq. (4) leads to a typical contact duration (half-period) $t_c \approx 2.27 \cdot 10^{-4}$ s, for a normal collision with $\gamma = 0$. Accordingly, an integration time-step of $t_{MD} = 2 \cdot 10^{-6}$ s is used, in order to allow for a ‘safe’ integration of contacts. Note that not only the normal ‘eigenfrequency’ but also the eigenfrequencies in tangential and rotation direction have to be considered as well as the viscous response times $t_\gamma \approx m/\gamma$. All of the eigenfrequencies should be considerably larger than t_{MD} , whereas the viscous response times should be even larger, so that $t_\gamma > t_c > t_{MD}$. The discussion of all the effects due to the interplay between the model parameters is far from the scope of this paper, however.

3.2 Compression simulations

When compressing the system (by growing the particles) the first quantity of interest is the density (volume fraction) ν . For a set of friction-

less hard spheres, the maximum volume fraction is $\nu_{max} \approx 0.74$, when all spheres are optimally arranged on a crystal lattice. Random packings can reach volume fractions between 0.63 and 0.69, dependent on the degree of local crystallization. When friction is switched on and also the other force laws are used, much smaller volume fractions are expected, see Fig. 3 below.

Before the results of the compression simulations can be discussed, one first needs a criterion whether a packing is stable and quasi-static or not. From one compression simulation, the ratio of kinetic to potential energy, $e = E_{kin}/E_{pot}$, and the coordination number (number of contacts per particle) are plotted in Fig. 2.

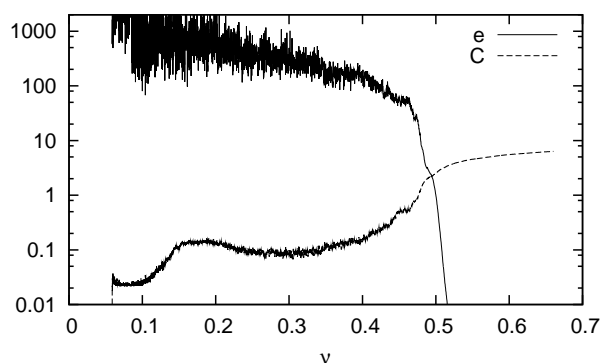


Figure 2: Energy ratio e and coordination number C plotted as function of the volume fraction during the continuous growth of the particles. The parameters are given in table 2.

Since the increase of C above two is correlated to the rapid drop of e below values of order unity, the densities are reported when $e = 1, 10^{-1}, 10^{-2}$, and 10^{-3} . For fixed friction coefficient, $\mu = 1$, see Fig. 3 (Top), increasing rolling- and torsion-coefficients lead to lower and lower densities. For the higher values of μ_r and μ_o , reorganization can appear more violently during ongoing compaction, leaving the system with somewhat higher density. For fixed finite rolling- and torsion coefficients, $\mu_r = \mu_o = 0.1$, see Fig. 3 (Bottom), the density is close to the reference without tangential forces and torques. With increasing friction coefficient μ the density drops. But the highest values of $\mu \geq 0.5$ do not necessarily lead to lower densities, as one could have expected. Again, the more violent reorganization events could be responsible.

Based on the variation of the friction-, rolling-, and torsion-coefficients, the lowest volume fraction to be expected for a stable packing can be extrapolated from Fig. 3 (Top) to be about $\nu_{min} \approx 0.42$. Too small friction coefficients are always related to rather high densities, and large friction alone

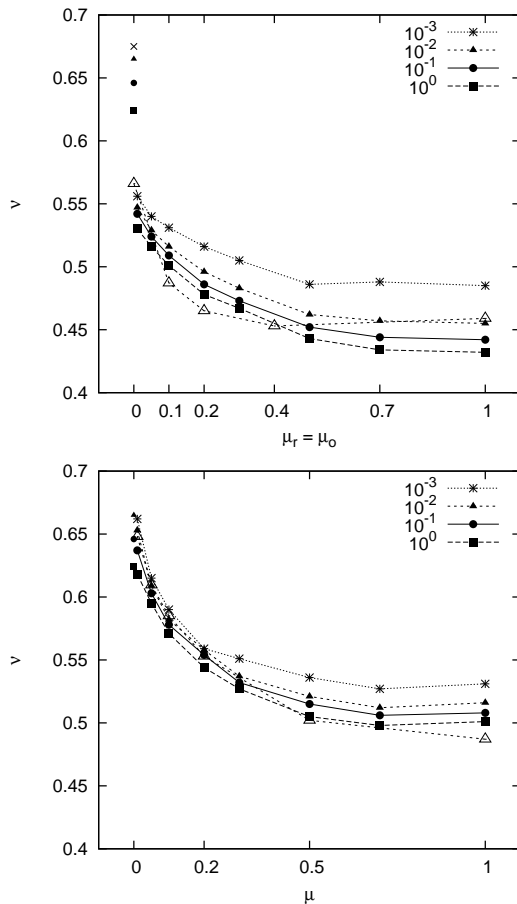


Figure 3: (Top) Densities (volume fractions) at which the energy ratio reaches the values e as given in the inset. The parameters are given in table 2, only the values of rolling- and torsion-coefficients are varied while $\mu = 1$ is kept constant. The lines are a guide to the eye and the points at top-left are the reference data for $\mu = \mu_r = \mu_o = 0$. (Bottom) Rolling and torsion-coefficients are fixed at $\mu_r = \mu_o = 0.1$ and the friction coefficient μ is varied. Lines and solid points are the same as in the top panel. For both panels, the open triangles are the data from Ref. [20], where Eq. (18) was used, while in this study, Eq. (19) is applied.

is not sufficient for low packing density: larger rolling and torsion resistance leads to smaller densities. On the other hand, extremely high friction-coefficients do not necessarily lead to lower densities due to a different reorganization dynamics.

3.3 Agglomeration with long range attraction

While a compaction procedure similar to the above was discussed in Ref. [20], the focus is here agglomeration, i.e., the formation of stable, low density clusters of adhesive, frictional particles – using all the interaction laws discussed before.

With some attractive long range force, the minimal packing density can be considerably decreased relative to the lowest densities achieved with contact forces only [20]. Due to the attractive forces, small clusters form, collide with each other and

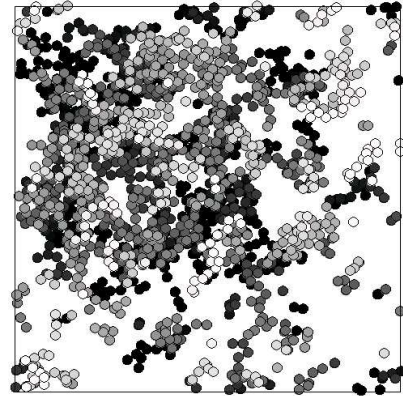


Figure 4: Snapshot from a simulation with long range attractive forces at volume fraction $\nu = 0.21$. The agglomerate is stable at this density, but does not fill the complete system. The greyscale indicates the distance from the viewer – more distant particles are darker. The lines indicate the (periodic) boundary of the system.

form larger, fractal-like structures, see Fig. 4. The attractive forces and the contact forces *together* stabilize the agglomerate structure.

4 Conclusion

The present study is a summary of the soft particle force models involving elastic-plastic contact deformation, adhesion, friction, and rolling- as well as torsion resistance. On top, a longer ranged attractive potential (like van der Waals) can be superposed, leading to stable fractal-like agglomerate structures. A set of exemplary parameters is given and several criteria and rules for parameter selection are discussed. Using friction and rolling-/torsion-resistance, stable static packings could be reached with rather low densities (volume fractions), somewhat above $\nu_{\min} \approx 0.4$. When also an attractive, longer ranging force was added, the minimal possible density was in the range from 0.2 to 0.4, but more systematic studies are needed here.

The set of contact models presented – even though many simplifying model assumptions are made – still involves a rather large number of parameters. Some of them are less important for physical properties and behavior of the system than others – the latter, most relevant parameters have to be identified and their interplay has to be better understood. Eventually, the validation of the simulation contact models and the corresponding parameters the issue.

The measurement of low packing fractions in adhesive, frictional fine powders is one of the pos-

sible experiments to be examined in more detail – a challenge for particle contact modeling. The qualitative particle-modeling approach of the early years has developed into the attempt of *quantitative* predictive modeling.

Acknowledgements

Valuable discussions with the project partners (H.-J. Butt, M. Kappl, J. Tomas, and R. Tykhoniuk) are acknowledged as well as the detailed communication with Danie Els about the objectivity of the model forces and torques. Furthermore, we acknowledge the financial support of the Deutsche Forschungsgemeinschaft (DFG) and the Stichting voor Fundamenteel Onderzoek der Materie (FOM), financially supported by the Nederlandse Organisatie voor Wetenschappelijk Onderzoek (NWO).

References

- [1] M. P. Allen and D. J. Tildesley. *Computer Simulation of Liquids*. Oxford University Press, Oxford, 1987.
- [2] F. Alonso-Marroquin, S. Luding, H. J. Herrmann, and I. Vardoulakis. Role of anisotropy in the elastoplastic response of a polygonal packing. *Phys. Rev. E*, 71:051304–(1–18), 2005.
- [3] G. Bartels, T. Unger, D. Kadau, D. E. Wolf, and J. Kertesz. The effect of contact torques on porosity of cohesive powders. *Granular Matter*, 7:139, 2005.
- [4] Y. M. Bashir and J. D. Goddard. A novel simulation method for the quasi-static mechanics of granular assemblages. *J. Rheol.*, 35(5):849–885, 1991.
- [5] P. A. Cundall and O. D. L. Strack. A discrete numerical model for granular assemblies. *Géotechnique*, 29(1):47–65, 1979.
- [6] C. T. David, R. Garcia-Rojo, H. J. Herrmann, and S. Luding. Powder flow testing with 2d and 3d biaxial and triaxial simulations. *Journal of Particle and Particle System Characterization*, in press, 2006.
- [7] C. T. David, R. G. Rojo, H. J. Herrmann, and S. Luding. Hysteresis and creep in powders and grains. In R. Garcia-Rojo, H. J. Herrmann, and S. McNamara, editors, *Powders and Grains 2005*, pages 291–294, Leiden, Netherlands, 2005. Balkema.
- [8] E. Dintwa, M. van Zeebroeck, E. Tijskens, and H. Ramon. Torsion of viscoelastic spheres in contact. *Granular Matter*, 7:169, 2005.
- [9] D. Els. Definition of roll velocity for spherical particles. preprint, 2006.
- [10] H. J. Herrmann, J.-P. Hovi, and S. Luding, editors. *Physics of dry granular media - NATO ASI Series E 350*, Dordrecht, 1998. Kluwer Academic Publishers.
- [11] M. Kappl, L. Heim, H.-J. Butt, S. Luding, R. Tykhoniuk, and J. Tomas. From grains to powders: from single particle contact mechanics measurements to bulk powder properties. In R. Garcia-Rojo, H. J. Herrmann, and S. McNamara, editors, *Powders and Grains 2005*, pages 493–497, Leiden, Netherlands, 2005. Balkema.
- [12] M. Lätzel, S. Luding, H. J. Herrmann, D. W. Howell, and R. P. Behringer. Comparing simulation and experiment of a 2d granular couette shear device. *Eur. Phys. J. E*, 11(4):325–333, 2003.
- [13] S. Luding. Collisions & contacts between two particles. In H. J. Herrmann, J.-P. Hovi, and S. Luding, editors, *Physics of dry granular media - NATO ASI Series E350*, page 285, Dordrecht, 1998. Kluwer Academic Publishers.
- [14] S. Luding. Micro-macro models for anisotropic granular media. In P. A. Vermeer, W. Ehlers, H. J. Herrmann, and E. Ramm, editors, *Modelling of Cohesive-Frictional Materials*, pages 195–206, Leiden, Netherlands, 2004. Balkema. (ISBN 04 1536 023 4).
- [15] S. Luding. Micro-macro transition for anisotropic, frictional granular packings. *Int. J. Sol. Struct.*, 41:5821–5836, 2004.
- [16] S. Luding. Molecular dynamics simulations of granular materials. In H. Hinrichsen and D. E. Wolf, editors, *The Physics of Granular Media*, pages 299–324, Weinheim, Germany, 2004. Wiley VCH.
- [17] S. Luding. Anisotropy in cohesive, frictional granular media. *J. Phys.: Condens. Matter*, 17:S2623–S2640, 2005.
- [18] S. Luding. The micro-macro mechanics of granular materials. *GACM report*, 2:22–28, 2005.
- [19] S. Luding. Shear flow modeling of cohesive and frictional fine powder. *Powder Technology*, 158:45–50, 2005.

- [20] S. Luding. Contact models for very loose granular materials. IUTAM Proceedings, submitted, 2006.
- [21] S. Luding, E. Clément, A. Blumen, J. Rajchenbach, and J. Duran. Anomalous energy dissipation in molecular dynamics simulations of grains: The “detachment effect”. *Phys. Rev. E*, 50:4113, 1994.
- [22] S. Luding, E. Clément, A. Blumen, J. Rajchenbach, and J. Duran. The onset of convection in molecular dynamics simulations of grains. *Phys. Rev. E*, 50:R1762, 1994.
- [23] S. Luding and H. J. Herrmann. Micro-macro transition for cohesive granular media. in: Bericht Nr. II-7, Inst. für Mechanik, Universität Stuttgart, S. Diebels (Ed.), 2001.
- [24] S. Luding, K. Manetsberger, and J. Muellers. A discrete model for long time sintering. *Journal of the Mechanics and Physics of Solids*, 53(2):455–491, 2005.
- [25] S. Luding, K. Manetsberger, and J. Müllers. A discrete model for long time sintering. submitted, 2004.
- [26] S. Luding, R. Tykhoniuk, and J. Tomas. Anisotropic material behavior in dense, cohesive powders. *Chem. Eng. Technol.*, 26(12):1229–1232, 2003.
- [27] D. C. Rapaport. *The Art of Molecular Dynamics Simulation*. Cambridge University Press, Cambridge, 1995.
- [28] M. H. Sadd, Q. M. Tai, and A. Shukla. Contact law effects on wave propagation in particulate materials using distinct element modeling. *Int. J. Non-Linear Mechanics*, 28(2):251, 1993.
- [29] C. Thornton. Numerical simulations of deviatoric shear deformation of granular media. *Géotechnique*, 50(1):43–53, 2000.
- [30] C. Thornton and L. Zhang. A dem comparison of different shear testing devices. In Y. Kishino, editor, *Powders & Grains 2001*, pages 183–190, Rotterdam, 2001. Balkema.
- [31] J. Tomas. Particle adhesion fundamentals and bulk powder consolidation. *KONA*, 18:157–169, 2000.
- [32] R. Tykhoniuk, J. Tomas, and S. Luding. Shear dynamics simulations of high-disperse cohesive powders. In *Proceedings of: Particulate Systems Analysis*, pages 1–5, 2003. 10-12 Sept. 2003).
- [33] R. Tykhoniuk, J. Tomas, and S. Luding. Simulation of shear dynamics of cohesive powders. *Chem. Ing. Tech.*, 76:59–62, 2004.
- [34] R. Tykhoniuk, J. Tomas, S. Luding, M. Kappl, and H.-J. Butt. Flow behaviour of ultrafine cohesive powder: View from inside. World Congress Particle Technology, CD-Proceedings, 2006.
- [35] R. Tykhoniuk, J. Tomas, S. Luding, M. Kappl, L. Heim, and H.-J. Butt. Adhesion, inelastic contact behavior and simulation of shear dynamics of ultrafine cohesive powder. In R. Garcia-Rojas, H. J. Herrmann, and S. McNamara, editors, *Powders and Grains 2005*, pages 499–503, Leiden, Netherlands, 2005. Balkema.
- [36] P. A. Vermeer, S. Diebels, W. Ehlers, H. J. Herrmann, S. Luding, and E. Ramm, editors. *Continuous and Discontinuous Modelling of Cohesive Frictional Materials*, Berlin, 2001. Springer. Lecture Notes in Physics 568.
- [37] O. R. Walton and R. L. Braun. Viscosity, granular-temperature, and stress calculations for shearing assemblies of inelastic, frictional disks. *J. Rheol.*, 30(5):949–980, 1986.
- [38] C. Y. Zhu, A. Shukla, and M. H. Sadd. Prediction of dynamic contact loads in granular assemblies. *J. of Applied Mechanics*, 58:341, 1991.